Prograde amphibole dehydration reactions during high-grade regional metamorphism, central Massachusetts, U.S.A.

Kurt Hollocher

Geology Department, Union College, Schenectady, New York 12308, U.S.A.

Abstract

The study area extends for 80 km through regionally metamorphosed rocks in the metamorphic high of southern New England, in which Acadian (Devonian) metamorphism ranged from sillimanite-muscovite grade through sillimanite-garnet-cordierite-orthoclase grade. Over this metamorphic interval, amphibolites containing the assemblages plagioclase + hornblende ± quartz ± cummingtonite ± orthoamphibole ± garnet were transformed by a series of reactions into pyroxene granulites with assemblages of plagioclase + orthopyroxene + augite ± quartz ± hornblende ± garnet. Three particularly important reactions were examined in detail. These reactions, along with others, define an assemblage series in quartz-bearing rocks in the transition from amphibolite facies to granulite facies. This assemblage series, listed below, is based on the coexistence of diagnostic minerals in common mafic rocks with increasing grade.

hornblende + orthoamphibole assemblage (Mg-rich rocks only)

orthoamphibole + hornblende + quartz = cummingtonite + plagioclase + H_2O

hornblende + cummingtonite assemblage

cummingtonite + plagioclase = hornblende + orthopyroxene + quartz + H_2O
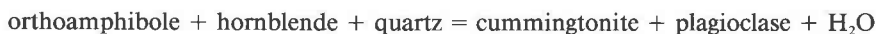
hornblende + orthopyroxene assemblage

hornblende + quartz = augite + orthopyroxene + plagioclase + H_2O

orthopyroxene + augite assemblage.

This transition is estimated to have occurred over a temperature interval of 580–730 °C.

Introduction

The progression of amphibole dehydration reactions was characterized for common amphibolites in the high-grade metamorphic rocks of Acadian (Devonian) age of central Massachusetts. In the western part of the area, the Bronson Hill anticlinorium (Fig. 1A) is the primary structural feature, a north trending belt of structural domes of Acadian age. The domes have abundant metamorphosed igneous rocks of Ordovician age exposed in their cores, with late Precambrian rocks also exposed in the Pelham Dome (Fig. 1; Robinson et al., 1989). The older rocks in the dome cores are overlain by a stratified sequence of metamorphosed sedimentary and volcanic rocks of Ordovician, Silurian, and Devonian ages. In the eastern part of the area, the Merrimack synclinorium is the primary structural feature, a thick sequence of Silurian and Devonian metamorphosed sedimentary rocks and possibly older basement gneisses (Berry, 1988).

The rocks were intruded by plutons, intensely deformed, and regionally metamorphosed to granulite facies during the Acadian Orogeny (Zen, 1983; Robinson, 1983; Robinson et al., 1986). The transition in mafic rocks

from amphibolites to pyroxene granulites is gradual and pervasive, and it is not associated with veins or individual plutons. Medium- and high-grade metamorphic rocks in southern New England have been subdivided into six metamorphic zones that are based on assemblages in pelitic schists: Zone I, kyanite + muscovite + staurolite; Zone II, sillimanite + muscovite + staurolite; Zone III, sillimanite + muscovite; Zone IV, sillimanite + muscovite + orthoclase; Zone V, sillimanite + orthoclase; and Zone VI, sillimanite + orthoclase + garnet + cordierite (Tracy et al., 1976). Isotherms estimated for prograde metamorphism are shown in Figure 1B. Temperature estimates for the samples analyzed based on these isotherms range from about 580 °C, in lower metamorphic Zone II, up to 730 °C in Zone VI (Table 1). The temperature estimates in Figure 1B and Table 1 are probably fairly precise relative to each other (with a few exceptions) but are probably accurate to no better than ±50 °C. Estimated prograde metamorphic pressures in the region are about 6 kbar (Tracy et al., 1976; Hollocher, 1981; Robinson et al., 1982b).

This study complements previous petrographic investigations of metamorphosed mafic rocks in southern New
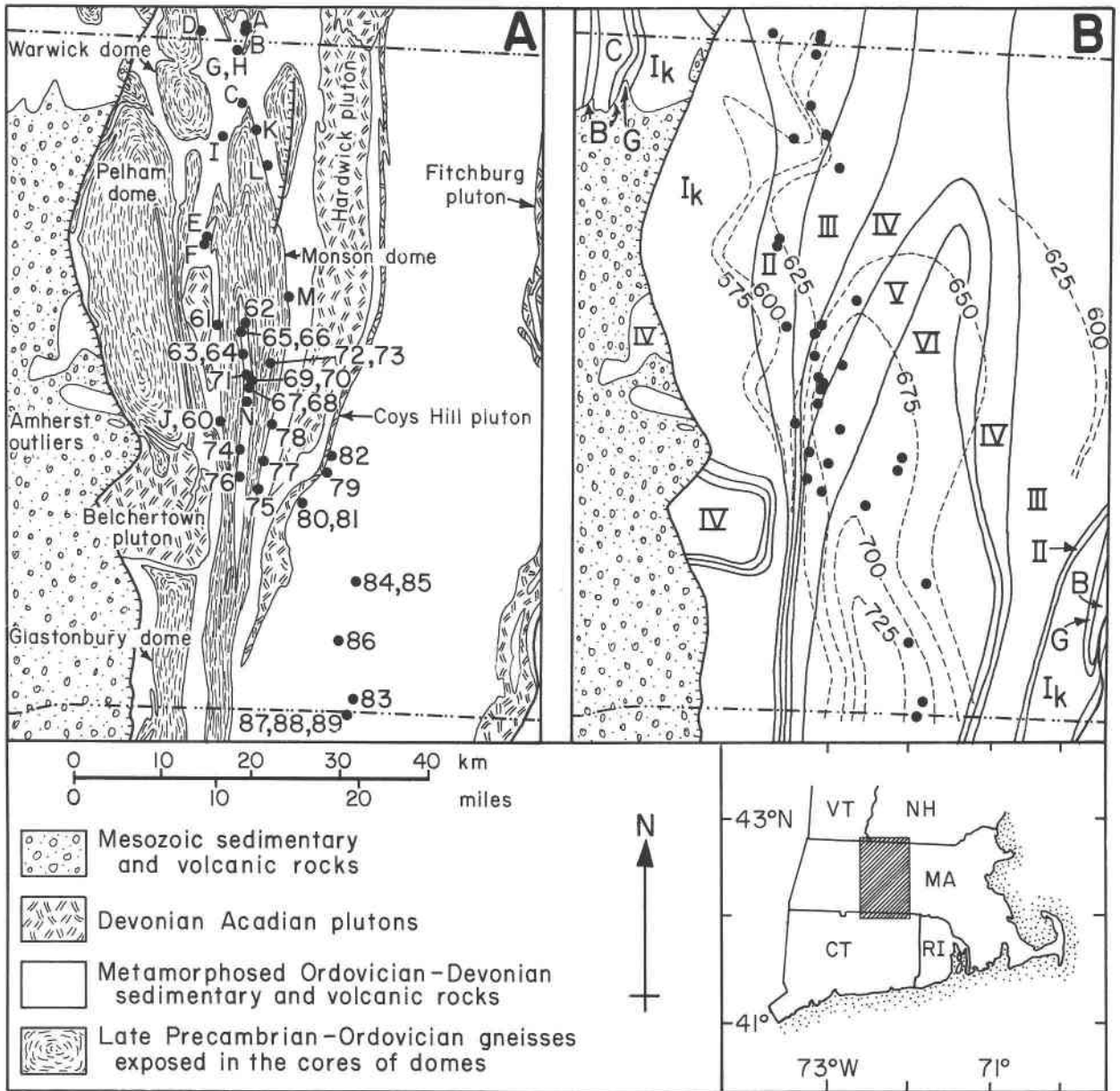
Fig. 1. (**A**) Simplified geologic map showing sample locations (map after Zen, 1983). (**B**) Metamorphic isograds for Zones I through VI, after Zen (1983). Superimposed on the isograds are metamorphic isotherms (from Robinson et al., 1982b; based on garnet-biotite geothermometry in schists from Tracy et al., 1976).

England, which have concentrated on phase relations in metamorphic Zones I–IV, and extends work to Zones V and VI (Robinson and Jaffe, 1969; Robinson et al., 1969 and 1971b; Huntington, 1975; Wolff, 1978; Robinson and Tracy, 1979; Schumacher, 1983; Hollocher, 1984; Schumacher and Robinson, 1987). This work also builds on the work of others in New England (e.g., Spear, 1978, 1980, 1982; Laird, 1980) and elsewhere.

SAMPLES AND METHODS

About 200 fresh amphibole- and pyroxene-bearing rocks were collected from layered and massive amphib-

olites, ultramafic rocks, pyroxene granulites, and Fe-rich granulites in central Massachusetts, southwestern New Hampshire, and north-central Connecticut. Rocks with assemblages containing the prograde calcareous minerals calcite, epidote, titanite, or clinopyroxene, in the absence of the Fe-Mg minerals garnet, cummingtonite, orthoamphibole, and orthopyroxene, were excluded from this study. Most of the rocks analyzed are hornblende bearing and have intermediate bulk X_{Mg} [Mg/(Mg + Fe^{2+})] of 0.4–0.7. Many of these rocks, including some with Fe-Mg amphibole, have essentially igneous compositions that are similar to basalts and mafic diorites. Other samples have

TABLE 1. Sample modes, feldspar compositions, and estimated metamorphic temperatures

| | Zone II | | Zone IV | | | | | | | | | | | |
Sample no.	60	61	62	63	64	65a	65b	66a	66b	67	68	69	70	71
Quartz				41		2	15			5			10	15
Plagioclase	43	50	49		40	66	64	42	44	47	14	62	38	37
Orthoclase														
Hornblende	35	46	30	tr R	49	15	1 R	25	2	15	85	25	20	35
Cummingtonite	20	3	15	20	5	15	15			25		10	20	5
Gedrite								30	30		1			
Anthophyllite			5		4		3		20					
Biotite	tr		tr		tr	tr	1	2	3	5	tr	3	1	1
Garnet				35									10	6
Augite														
Orthopyroxene														
Ilmenite	2	tr	1	1	2	2	1	tr	tr R	1	tr	tr	1	1
Magnetite										2				
Spinel														
Rutile		tr	tr R		tr R		tr	1	1		tr R	tr		tr R
Zircon	tr	tr	tr	tr	tr	tr	tr			tr	tr		tr	tr
Apatite	tr	tr	tr	3	tr	tr	tr	tr	tr	tr	tr	tr	tr	tr
Allanite	tr			tr									tr	
Pyrite							tr R			tr R				
Pyrrhotite			tr	tr		tr		tr			tr			tr
Chalcopyrite											tr			
Chlorite		1 R		tr R		tr	tr R	tr R	tr R	tr R				
Talc		tr R						tr R	tr R					
Sericite	tr R		tr R		tr R		tr R	tr R	tr R	tr R		tr R	tr R	tr R
Calcite														
Serpentine														
Total	100	100	100	100	100	100	100	100	100	100	100	100	100	100
An in plag.	40.1	79.8	25.1		30.5	34.4	27.7	42.9	39.7	40.6	85.4	73.7	41.8	36.7
Or in potassium feldspar														
Estimated T**	635	605	645	655	655	630	630	630	630	685	685	685	685	675

Note: Samples 78 and 89 contain trace sillimanite in garnet, which is probably not part of the bulk assemblage. Sample 74a contains trace covellite, which is probably a weathering product. See Appendix 1 for samples A–N. Abbreviations: tr = trace amounts present, generally ≪1%; R = mineral is of retrograde origin.
 * Poor control for these estimated temperatures.
 ** Estimated temperatures derived from Figure 1B.

altered igneous or nonigneous compositions (Schumacher, 1983; Hollocher, 1985).

From 151 of the collected samples, 172 thin sections were made and 30 thin sections containing 33 distinct prograde mineral assemblages (samples 60–89) were selected for detailed study (Table 1). The 33 assemblages were studied using reflected and transmitted light microscopes and analyzed by electron microprobe (samples 60–89; see Hollocher, 1985, for detailed sample descriptions, sample locations, and analytical procedures). Representative analyses of selected samples are given in Tables 2–5.[1] Complementing these samples are data from 14 previously published amphibole-bearing assemblages in central Massachusetts and southwestern New Hampshire (samples A–N, see Appendix 2).

In Zones V and VI, some of the mafic rocks contain coarse-grained veins that are sharply crosscutting to dif-

fuse and have the same mineral content as the host rock, but in different modal proportions (e.g., samples 75 and 87). These veins appear to be locally derived partial melts of the host rock. The percentage of partial melting was apparently small (<5%) in most cases, and melting apparently did not proceed to the exhaustion of any phase. The effect of partial melting on amphibole phase relations is probably unimportant to the discussion below because the veins and their host rocks have evidence of strong subsolidus deformation and recrystallization. The assemblages probably represent true subsolidus metamorphic assemblages that last equilibrated in the absence of silicate liquid.

Petrography

Hornblende

Prograde hornblende occurs as olive green to brown, stubby to elongate crystals. Hornblende in equilibrium with cummingtonite contains colorless cummingtonite exsolution lamellae that are also common in hornblende from cummingtonite-free assemblages (see Jaffe et al., 1968, and Robinson et al., 1971a, for a discussion). Blue-green retrograde hornblende that is Na-rich, Fe-rich, and Ti-poor occurs as thin rims or tiny grains surrounding

TABLE 1—*Continued*

Zone V								Zone VI										
72	73	74a	74b	75	76	77	78	79	80	81	82	83	84	85	86	87	88	89
		20	2	15	15			tr	2	5			3	15	15	2	20	tr R
22	44	62	54	54	52	47	70	18	46	56	29	45	65	73	51	67	61	55
										tr				3		tr	1	
54	7	2	40	25	15			10	40	10	5	46	15	tr R	15	tr R		
tr		5	3	tr R	10	tr R	1		tr R		3	tr R		tr R		tr R	tr R	1 R
23	15					30	10											2
tr	2			tr R	5	2	2	7	1	5	2	2	2	2	1	5	7	15
tr	30				3	5	15			5				2			5	2
										1		tr	3		2	15		
		10		3		15	1	65	7	10	60	7	10	5	15	10	5	25
1	1	tr	1	1	tr R	1	1	tr R	2	2	tr	tr	1	tr R	tr	1	tr R	tr
tr	1	1		2														
tr	tr																	
	tr																	
tr	tr	tr	tr	tr	tr	tr	tr	tr	tr	tr		tr	tr	tr	tr	tr		tr
tr	tr	tr	tr	tr	tr	tr	tr	tr	1	2	tr	tr	1	tr		tr	1	tr
										tr						tr		
		tr R		tr				tr	tr R	tr R		tr R	tr R	tr R	tr R			tr R
	tr	tr		tr	tr				tr	tr	1	tr	tr	tr	1	tr	tr	tr
		tr		tr	tr						tr	tr	tr	tr			tr	tr
	tr R									tr R	tr R			tr R	tr R			tr R
											tr R							
tr R	tr R		tr R	tr R	tr R	tr R	tr R		tr R	tr R	tr R	tr R	tr R	tr R		tr R	tr R	tr R
								tr R		tr R	tr R			tr R	tr R			tr R
										tr R				tr R				
100	100	100	100	100	100	100	100	100	100	100	100	100	100	100	100	100	100	100
41.4	42.9	25.0	25.0	26.6	41.2	26.1	15.2	87.1	41.5	44.2	51.0	47.2	46.6	32.7	49.3	43.5	27.0	47.4
														92.1	85.0	85.2		
690	690	660	660	670	655	680	690	685	695	695	680	710	660*	660*	705	715	715	715

prograde hornblende, contrasting with light green actinolitic hornblende that is retrograde after augite. Representative hornblende analyses are given in Table 2.

Cummingtonite

Prograde cummingtonite is colorless to pale green in thin section and is generally untwinned. It contains abundant green hornblende exsolution lamellae. In contrast, fine-grained retrograde cummingtonite after orthopyroxene has fine-scale polysynthetic twinning and no visible exsolution lamellae. Representative cummingtonite analyses are given in Table 3.

Orthoamphibole

In thin section, anthophyllite is colorless to very pale pink or tan. In Zones I–IV, gedrite is pink to pinkish brown in magnetite-free rocks and gray-green in magnetite-bearing rocks, but is brown in Zones V and VI regardless of the presence of magnetite. Gedrite in anthophyllite-, cummingtonite-, or hornblende-bearing assemblages typically has fine-scale {010} exsolution lamellae of anthophyllite, whereas anthophyllite has no visible lamellae. Representative orthoamphibole analyses are given in Table 3.

Pyroxene

Augite occurs as blocky crystals that are colorless to faint green in thin section. The augite contains pigeonite exsolution lamellae on irrational planes close to {001} and {100} and commonly contains lamellae of orthopyroxene on {100} (see Jaffe et al., 1975, and Robinson et al., 1971a and 1977, for discussions). Orthopyroxene is colorless or pleochroic faint green to pale pink and, in augite-bearing assemblages, has clinopyroxene exsolution lamellae on {100}. Orthopyroxene has only 0.4 to 3.8% of diopside-hedenbergite component, and nonquadrilateral components vary from 2.2 to 6.4% in quartz-bearing assemblages and up to 11.3% in quartz-free assemblages. Representative pyroxene analyses are given in Table 4.

Garnet

Garnet occurs as 1–5 mm equant euhedral to anhedral grains. In contrast to the strongly zoned garnet that is typical of pelitic rocks in the area (e.g., Tracy et al., 1976), most garnet in the amphibolites and pyroxene granulites is unzoned within analytical uncertainty. The complete range of garnet compositions is almandine 57–69%, pyrope 11–31%, grossular 2–20%, and spessartine 2–16% (Table 4). Representative garnet analyses are given in Table 5.

Feldspar

Plagioclase compositions are in the range of An_{15}–An_{87} and $Or_{0.1}$–$Or_{2.0}$ for all samples (Table 1). Plagioclase in several samples is zoned, with sparse calcic cores in sharp contact with nearly homogeneous sodic rims. The calcic cores are probably igneous or early metamorphic relics that never recrystallized during high-grade metamor-

TABLE 2. Electron probe analyses and structural formulae of hornblende

| Sample: | 65a | 67 | 70 | 74a | 75 | 76 | 79 | 81 | 82 | 84 | 86 |
n	19	15	10	6	10	15	30	17	8	10	20
SiO_2	46.20	44.29	44.46	42.96	45.97	45.65	54.02	42.03	49.27	46.49	43.87
TiO_2	0.78	0.77	1.15	0.89	1.34	1.17	0.40	1.87	1.33	1.94	1.51
Al_2O_3	10.50	12.51	11.74	11.63	8.84	10.55	5.41	11.50	8.65	9.06	10.81
Fe_2O_3	4.28	4.89	3.05	5.98	4.19	1.74	0.93	2.50	1.12	2.11	4.57
FeO	10.88	12.72	16.48	16.22	13.24	15.85	4.67	18.89	9.10	12.11	12.16
MnO	0.32	0.14	0.11	0.38	0.45	0.20	0.12	0.18	0.22	0.25	0.51
MgO	13.38	11.43	9.69	8.45	11.84	9.97	20.05	6.99	15.78	12.51	11.18
CaO	9.88	9.51	9.57	9.69	10.34	10.69	11.83	11.07	10.48	11.29	11.49
Na_2O	1.55	1.26	1.36	1.97	1.77	1.41	0.53	1.44	1.20	1.28	1.29
K_2O	0.24	0.25	0.39	0.42	0.34	0.55	0.16	1.41	0.31	0.84	0.98
Cl				0.01	0.00						
Total	98.01	97.77	98.00	98.60	98.32	97.78	98.12	97.88	97.46	97.88	98.37
	Structural formulae calculated to 23 O atoms (see below for Fe^{3+} correction type)										
Si	6.703	6.499	6.598	6.432	6.759	6.768	7.465	6.421	7.038	6.804	6.479
Al	1.297	1.501	1.402	1.568	1.241	1.232	0.535	1.579	0.962	1.196	1.521
[4]Sum	8.000	8.000	8.000	8.000	8.000	8.000	8.000	8.000	8.000	8.000	8.000
Al	0.498	0.663	0.651	0.484	0.291	0.611	0.346	0.492	0.494	0.367	0.361
Fe^{3+}	0.467	0.540	0.341	0.674	0.464	0.194	0.097	0.287	0.120	0.232	0.508
Ti	0.085	0.085	0.128	0.100	0.148	0.130	0.042	0.215	0.143	0.214	0.168
Mg	2.894	2.500	2.144	1.886	2.595	2.204	4.130	1.592	3.360	2.729	2.461
Fe^{2+}	1.056	1.212	1.736	1.856	1.502	1.861	0.385	2.413	0.883	1.458	1.502
Mn	0.000	0.000	0.000	0.000	0.000	0.000	0.000	0.001	0.000	0.000	0.000
[6]Sum	5.000	5.000	5.000	5.000	5.000	5.000	5.000	5.000	5.000	5.000	5.000
Fe^{2+}	0.264	0.349	0.309	0.175	0.126	0.104	0.155	0.000	0.204	0.024	0.000
Mn	0.039	0.017	0.014	0.048	0.056	0.025	0.014	0.022	0.027	0.031	0.064
Ca	1.536	1.495	1.521	1.554	1.629	1.698	1.751	1.812	1.604	1.770	1.818
Na	0.161	0.139	0.156	0.223	0.189	0.173	0.080	0.166	0.165	0.175	0.118
[M4]Sum	2.000	2.000	2.000	2.000	2.000	2.000	2.000	2.000	2.000	2.000	2.000
Na	0.275	0.219	0.235	0.349	0.316	0.232	0.062	0.261	0.167	0.188	0.251
K	0.044	0.047	0.074	0.080	0.064	0.104	0.028	0.275	0.056	0.157	0.185
[A]Sum	0.319	0.266	0.309	0.429	0.380	0.336	0.090	0.536	0.223	0.345	0.436
Total	15.319	15.266	15.309	15.429	15.380	15.336	15.090	15.536	15.223	15.345	15.436
Cl				0.002							
Correction type	A	A	A	A	A	A	0.15	13CAT	0.1	A	13CAT
Fe^{3+}/Fe_{tot}	0.261	0.257	0.143	0.249	0.222	0.090	0.152	0.106	0.099	0.135	0.253
$Mg/(Mg + Fe_{tot})$	0.618	0.543	0.473	0.411	0.554	0.505	0.866	0.371	0.736	0.614	0.550
$Mg/(Mg + Fe^{2+})$	0.687	0.616	0.512	0.481	0.614	0.529	0.884	0.398	0.756	0.648	0.621
$Mg/(Mg + Fe^{2+} + Mn)$	0.680	0.613	0.510	0.476	0.606	0.526	0.882	0.395	0.751	0.643	0.611
$Ca/(Ca + Na)$	0.779	0.807	0.796	0.731	0.763	0.807	0.925	0.809	0.829	0.830	0.831

phism and deformation. In sample 69 the calcic cores have unmixed into parallel lamellae of two plagioclase phases. Discrete crystals of orthoclase occur in samples 85 and 88; orthoclase also occurs as large, rectangular exsolution lamellae in plagioclase in samples 81 and 87. Orthoclase has a composition range of $Or_{85.0}–Or_{92.3}$, $An_{0.1}–An_{0.4}$, and $Cn_{1.1}–Cn_{4.9}$ (Table 1).

CALCULATION OF Fe^{3+} FROM ELECTRON PROBE ANALYSES

Review

The problem of calculating Fe^{3+} from electron probe analyses in nonstoichiometric minerals has been discussed extensively elsewhere (e.g., Robinson et al., 1982a, for amphibole; Dymek, 1983, for biotite). Figure 2 illustrates how important it is that some reasonable estimate of Fe^{3+} in amphibole be made. In Figure 2A the plotted cummingtonite and hornblende formulae have been calculated with all Fe as Fe^{2+}. Because the amphibole samples must have had differing quantities of Fe^{3+} initially, calculating all Fe as Fe^{2+} causes the plotted amphibole positions to shift from their true positions by varying amounts. The differential movement in plotted amphi-

bole positions results in chaotic crossing of cummingtonite-hornblende tie lines, with tie lines having both positive and negative slopes. Calculating all Fe as Fe^{2+} also increases the number of cations in the 23 O atom formulae, forcing Ca into the A site in many cases. This is a violation of an empirical crystal-chemical limit for common calcic amphibole (Robinson et al., 1982a). In Figure 2B the data were recalculated with an Fe^{3+} correction (Tables 2 and 3; except data from analysis of sample B, which is a wet chemical analysis). After correction, no Ca is assigned to A sites and all tie lines have positive slopes with more Na assigned to hornblende M(4) sites than to M(4) sites in coexisting cummingtonite, as expected.

The plotting parameter $(Na + K) − (\Sigma \text{ cations} − 15)$ in Figure 2 is particularly sensitive to the Fe^{3+} correction, but other parameters such as X_{Mg} are sensitive also. Using the proper Fe^{3+} correction is therefore important for the interpretation of data in phase diagrams and for calculating reaction coefficients. Fe^{3+} in amphibole was estimated in different ways for different samples (Tables 2 and 3) because no single calculation scheme worked for all analyses. Although selection of correction type is in part subjective, the resulting amphibole structural for-

TABLE 3. Electron probe analyses and structural formulae of cummingtonite and orthoamphiboles

	Cummingtonite								Orthoamphiboles	
Sample:	63	65a	65b	67	70	74a	76	82	65b	89
n	10	10	11	15	11	6	11	9	15	10
SiO_2	52.00	53.84	54.50	52.54	51.47	51.24	53.03	55.09	53.72	41.24
TiO_2	0.23	0.10	0.08	0.18	0.29	0.14	0.09	0.17	0.10	0.97
Al_2O_3	2.93	1.71	1.27	3.46	3.06	1.94	1.39	1.63	2.21	17.46
Fe_2O_3	2.14	1.94	0.80	1.88	1.26	2.30	0.46	0.41	1.41	2.44
FeO	20.37	18.62	19.27	20.92	24.90	26.09	25.47	17.10	18.51	17.83
MnO	1.44	0.74	0.80	0.31	0.30	0.78	0.44	0.43	0.80	0.38
MgO	16.82	19.60	19.93	17.52	14.14	13.80	15.59	21.44	20.55	13.99
CaO	1.60	1.26	0.91	1.42	2.07	1.25	1.20	1.22	0.53	0.78
Na_2O	0.45	0.24	0.16	0.38	0.40	0.34	0.14	0.15	0.31	2.34
K_2O	0.12	0.02	0.02	0.01	0.03	0.03	0.04	0.02	0.02	0.03
Cl	0.01					0.01				
Total	98.11	98.07	97.74	98.62	97.92	97.92	97.85	97.66	98.16	97.46
Structural formulae calculated to 23 O atoms (see below for Fe^{3+} correction type)										
Si	7.594	7.737	7.839	7.583	7.638	7.680	7.842	7.828	7.686	6.050
Al	0.406	0.263	0.161	0.417	0.362	0.320	0.158	0.172	0.314	1.950
[4]Sum	8.000	8.000	8.000	8.000	8.000	8.000	8.000	8.000	8.000	8.000
Al	0.098	0.027	0.054	0.172	0.173	0.023	0.084	0.101	0.059	1.069
Fe^{3+}	0.235	0.210	0.087	0.204	0.141	0.259	0.051	0.044	0.152	0.269
Ti	0.025	0.011	0.009	0.020	0.032	0.016	0.010	0.018	0.011	0.107
Mg	3.662	4.199	4.273	3.770	3.128	3.083	3.437	4.541	4.383	3.060
Fe^{2+}	0.980	0.553	0.577	0.834	1.526	1.619	1.418	0.296	0.395	0.495
[6]Sum	5.000	5.000	5.000	5.000	5.000	5.000	5.000	5.000	5.000	5.000
Fe^{2+}	1.508	1.685	1.741	1.691	1.564	1.651	1.732	1.736	1.820	1.693
Mn	0.178	0.090	0.097	0.038	0.038	0.099	0.055	0.052	0.097	0.047
Ca	0.250	0.194	0.140	0.220	0.329	0.201	0.190	0.186	0.081	0.123
Na	0.064	0.031	0.022	0.051	0.069	0.049	0.023	0.026	0.002	0.137
M4]Sum	2.000	2.000	2.000	2.000	2.000	2.000	2.000	2.000	2.000	2.000
Na	0.063	0.036	0.023	0.055	0.046	0.050	0.017	0.015	0.084	0.529
K	0.022	0.004	0.004	0.002	0.006	0.006	0.008	0.004	0.004	0.006
[A]Sum	0.085	0.040	0.027	0.057	0.052	0.056	0.025	0.019	0.088	0.535
Total	15.085	15.040	15.027	15.057	15.052	15.056	15.025	15.019	15.088	15.535
Cl	0.002					0.002				
Correction type	B	B	B	B	C	B	C	C	D	D
Fe^{3+}/Fe_{tot}	0.086	0.086	0.036	0.075	0.044	0.073	0.016	0.021	0.064	0.109
$Mg/(Mg + Fe_{tot})$	0.574	0.632	0.640	0.580	0.492	0.466	0.518	0.686	0.649	0.555
$Mg/(Mg + Fe^{2+})$	0.595	0.652	0.648	0.599	0.503	0.485	0.522	0.691	0.664	0.583
$Mg/(Mg + Fe^{2+} + Mn)$	0.579	0.643	0.639	0.595	0.500	0.478	0.517	0.685	0.655	0.578
$Ca/(Ca + Na)$	0.663	0.743	0.757	0.675	0.741	0.670	0.826	0.819	0.485	0.156

mulae violate no crystal-chemical limits, yield reasonably consistent sets of tie lines, and yield calculated reaction coefficients that agree qualitatively with petrographic evidence and interpretations of phase diagrams. The following is an explanation of the Fe^{3+} calculation schemes used.

Hornblende

A. Available wet chemical analyses of metamorphic hornblende in northern Massachusetts and southwestern New Hampshire have a remarkably consistent [A](Na + K)/(Na + K)$_{tot}$ ratio of about 0.66 (Robinson and Jaffe, 1969). This ratio was used for the Fe^{3+} correction for most hornblende analyzed in this study.

13CAT. The A correction failed because it put Ca into the M(1,2,3) sites, violating a crystal-chemical limit. The 13CAT correction yields nearly the maximum Fe^{3+} in which all cations excluding Mn, Ca, Na, and K total 13 (13eMnCNK scheme of Robinson et al., 1982a).

0.1. The formula calculated assuming all Fe as Fe^{2+} has a ratio of [A](Na + K)/(Na + K)$_{tot}$ < 0.66. Because zero Fe^{3+} is unlikely, an Fe^{3+}/Fe_{tot} ratio of 0.1 was assigned based on comparisons with hornblende from similar assemblages and metamorphic grade.
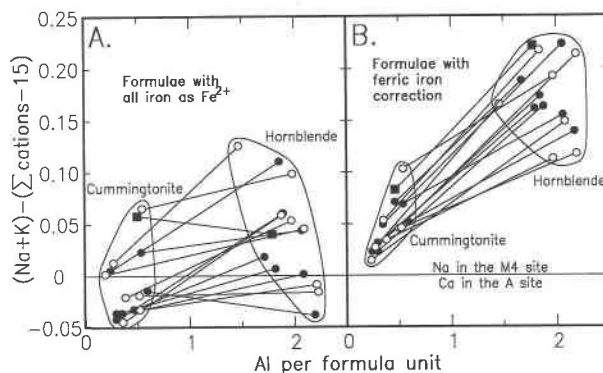

Fig. 2. Coexisting hornblende-cummingtonite pairs plotted with (Na + K) − (Σ cations − 15) vs. Al per formula unit, showing the differences between all Fe as Fe^{2+} amphibole formulae (**A**), and Fe^{3+} corrected amphibole formulae (**B**). Positive values of (Na + K) − (Σ cations − 15) equal the amount of Na assigned to M(4) sites (zero Ca in the A site). Negative values equal the amount of Ca assigned to the A site [zero Na in the M(4) site]. Closed symbols are for quartz-bearing and open symbols for quartz-free assemblages. Circles are data from this study, squares are a pair of wet chemical analyses from sample B (from Robinson and Jaffe, 1969).

TABLE 4. Electron probe analyses and structural formulae of pyroxene

	Augite			Orthopyroxene								
Sample:	81	84	86	74a	75	79	81	82	84	86	88	89
n	8	10	13	6	6	9	12	6	11	10	12	9
SiO$_2$	50.58	52.38	51.64	50.10	51.69	55.33	49.47	53.26	51.88	51.20	50.77	50.15
TiO$_2$	0.15	0.21	0.17	0.09	0.09	0.05	0.09	0.12	0.09	0.08	0.09	0.09
Al$_2$O$_3$	1.11	1.09	1.32	0.91	0.79	0.85	0.48	1.34	0.65	0.66	2.18	4.71
Fe$_2$O$_3$	1.33	0.98	1.88	0.98	0.17	0.88	0.80	0.79	1.15	0.58	0.90	0.32
FeO	16.46	9.84	10.61	31.90	27.15	13.88	36.10	20.63	25.99	29.97	27.77	25.13
MnO	0.43	0.38	0.28	1.13	1.23	0.30	0.79	0.45	0.77	0.65	0.36	0.38
MgO	8.98	13.43	12.27	14.71	18.36	28.88	11.98	23.70	19.17	16.67	18.09	19.22
CaO	20.52	21.47	21.56	0.53	0.58	0.36	0.77	0.31	0.83	0.65	0.19	0.17
Na$_2$O	0.30	0.23	0.33	0.02	0.00	0.02	0.00	0.01	0.02	0.03	0.03	0.02
Total	99.86	100.01	100.06	100.37	100.06	100.55	100.48	100.61	100.55	100.49	100.38	100.19
Structural formulae calculated to six O atoms and four cations												
Si	1.962	1.965	1.951	1.962	1.977	1.970	1.974	1.957	1.967	1.975	1.937	1.889
Al	0.038	0.035	0.049	0.038	0.023	0.030	0.023	0.043	0.029	0.025	0.063	0.111
[4]Sum	2.000	2.000	2.000	2.000	2.000	2.000	1.997	2.000	1.996	2.000	2.000	2.000
Al	0.013	0.013	0.010	0.004	0.013	0.006	0.000	0.015	0.000	0.005	0.035	0.098
Fe^{3+}	0.039	0.028	0.053	0.029	0.005	0.024	0.024	0.022	0.033	0.017	0.026	0.009
Ti	0.004	0.006	0.005	0.003	0.003	0.001	0.003	0.003	0.003	0.002	0.003	0.003
Mg	0.519	0.751	0.691	0.859	0.979	0.969	0.713	0.960	0.964	0.959	0.936	0.890
Fe^{2+}	0.425	0.202	0.241	0.105	0.000	0.000	0.260	0.000	0.000	0.017	0.000	0.000
[M1]Sum	1.000	1.000	1.000	1.000	1.000	1.000	1.000	1.000	1.000	1.000	1.000	1.000
Mg	0.000	0.000	0.000	0.000	0.068	0.563	0.000	0.338	0.120	0.000	0.093	0.189
Fe^{2+}	0.109	0.107	0.094	0.940	0.869	0.413	0.945	0.634	0.824	0.950	0.886	0.791
Mn	0.014	0.012	0.009	0.037	0.040	0.009	0.027	0.014	0.025	0.021	0.012	0.012
Ca	0.853	0.863	0.873	0.022	0.024	0.014	0.033	0.012	0.034	0.027	0.008	0.007
Na	0.023	0.017	0.024	0.002	0.000	0.001	0.000	0.001	0.001	0.002	0.002	0.001
[M2]Sum	0.999	0.999	1.000	1.001	1.001	1.000	1.005	0.999	1.004	1.000	1.001	1.000
Total	3.999	3.999	4.000	4.001	4.001	4.000	4.002	3.999	4.000	4.000	4.001	4.000
Fe^{3+}/Fe$_{tot}$	0.068	0.083	0.137	0.027	0.006	0.055	0.020	0.034	0.039	0.017	0.029	0.011
Mg/(Mg + Fe^{2+})	0.493	0.708	0.673	0.451	0.546	0.788	0.372	0.672	0.568	0.498	0.537	0.577
Mg/(Mg + Fe^{2+} + Mn)	0.486	0.701	0.668	0.443	0.535	0.784	0.367	0.667	0.561	0.493	0.534	0.573
% wollastonite	44.4	44.6	45.8	1.1	1.2	0.7	1.7	0.6	1.7	1.4	0.4	0.4
% nonquad.	5.9	5.0	7.1	3.8	2.2	3.1	2.5	4.2	3.3	2.6	6.5	11.1

Note: % Wollastonite = 100Ca/(Ca + Mg + Fe^{2+} + Mn); % nonquadrilateral components = 100 (Al + Ti + Na + Fe^{3+})/2.

TABLE 5. Electron probe analyses and structural formulae of garnet

| Sample:	63	70			76	81	88	89		
		core	int.	rim				core	int.	rim
n	6	4	6	8	9	12	13	5	5	5
SiO$_2$	37.23	38.03	38.19	38.02	38.18	37.73	38.14	38.39	38.46	38.32
Al$_2$O$_3$	20.96	21.24	21.37	21.31	21.36	20.96	21.91	21.59	21.48	21.49
FeO	27.65	31.83	31.34	31.31	30.20	29.85	31.13	29.03	29.54	29.24
MnO	7.06	1.16	1.11	1.30	1.69	1.72	1.14	1.09	1.33	1.01
MgO	3.83	3.90	4.16	3.99	4.26	2.76	6.79	6.38	5.54	5.88
CaO	3.26	4.69	4.71	4.68	5.11	7.28	1.71	4.29	4.57	4.52
Total	99.99	100.85	100.88	100.61	100.80	100.30	100.82	100.77	100.92	100.46
Structural formulae calculated to 12 O atoms										
[4]Si	2.982	3.001	3.004	3.002	3.002	3.001	2.973	2.986	2.999	2.995
[6]Al	1.979	1.976	1.981	1.983	1.979	1.965	2.013	1.979	1.974	1.979
Fe	1.852	2.101	2.062	2.068	1.986	1.986	2.029	1.889	1.926	1.911
Mn	0.480	0.078	0.074	0.087	0.113	0.116	0.075	0.072	0.088	0.067
Mg	0.457	0.459	0.488	0.470	0.499	0.327	0.789	0.740	0.644	0.685
Ca	0.280	0.397	0.397	0.396	0.430	0.620	0.143	0.358	0.382	0.378
[8]Sum	3.069	3.035	3.021	3.021	3.028	3.049	3.036	3.059	3.040	3.041
Total	8.030	8.012	8.006	8.006	8.009	8.015	8.022	8.024	8.013	8.015
Mg/(Mg + Fe)	0.198	0.179	0.191	0.185	0.201	0.141	0.280	0.281	0.251	0.264
Mg/(Mg + Fe + Mn)	0.164	0.174	0.186	0.179	0.192	0.135	0.273	0.274	0.242	0.257
% almandine	60.3	69.2	68.3	68.5	65.6	65.1	66.8	61.8	63.4	62.8
% spessartine	15.6	2.6	2.4	2.9	3.7	3.8	2.5	2.4	2.9	2.2
% pyrope	14.9	15.1	16.2	15.6	16.5	10.7	26.0	24.2	21.2	22.5
% grossular	9.1	13.1	13.1	13.1	14.2	20.3	4.7	11.7	12.6	12.4
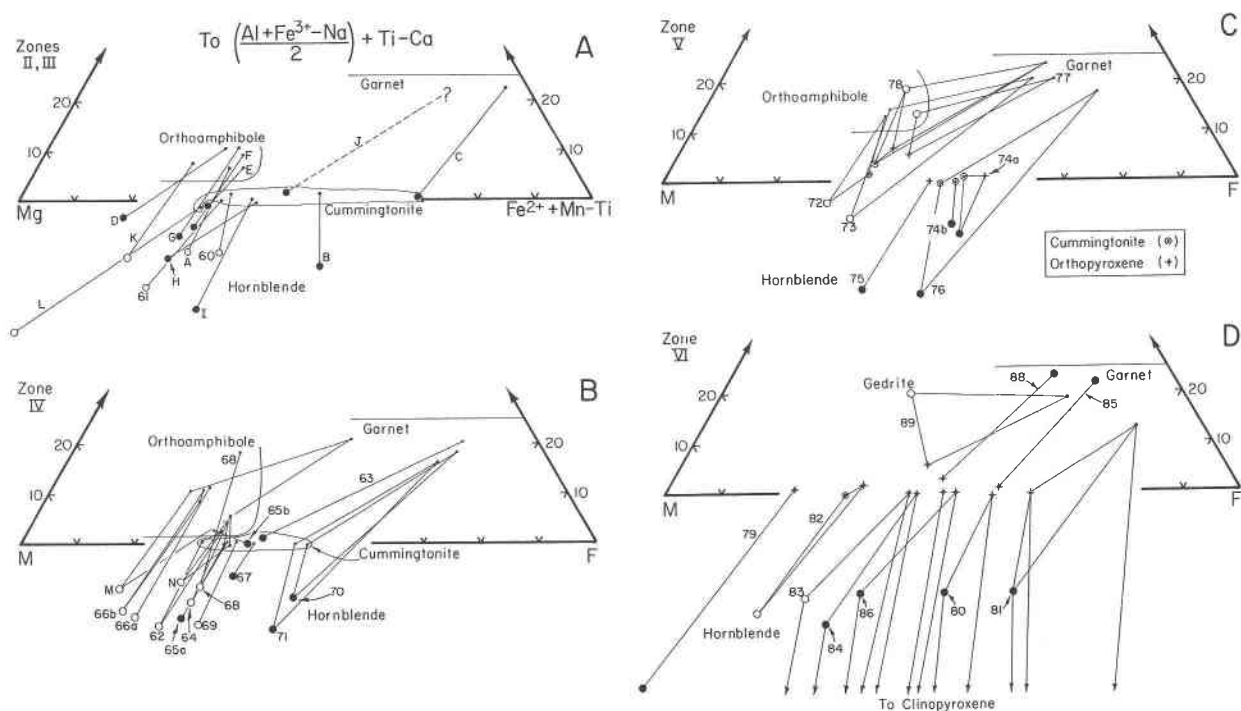
Fig. 3. Amphibole, garnet, and pyroxene data from all samples used in this study, shown projected onto the AFM ternary plane and separated according to metamorphic zone. Open symbols represent quartz-free assemblages and closed symbols represent quartz-bearing assemblages. For clarity, the symbols are shown only on hornblende or one other phase. In Figures 4C and 4D, cummingtonite is shown with dotted circles and orthopyroxene with crosses.

0.15. The ratio of Fe^{3+}/Fe_{tot} was calculated directly from available bulk rock analyses using X-ray fluorescence, wet chemical analyses, and modal analyses (Hollocher, 1985).

Cummingtonite

B. An average of the minimum Fe^{3+} correction (all cations excluding Na and K total 15; 15eNK) and the maximum correction (all cations excluding K totaled 15; 15eK).

C. An average of the minimum Fe^{3+} correction (all Fe as Fe^{2+}) and the maximum correction (all cations excluding K totaled 15; 15eK).

Orthoamphibole

D. Wet chemical analyses of metamorphic orthoamphiboles in southwestern New Hampshire and northern Massachusetts have a remarkably consistent $^{[Al]}(Na + K)/(Na + K)_{tot}$ ratio of about 0.79 (Robinson and Jaffe, 1969). This ratio was used for the Fe^{2+} for most orthoamphiboles analyzed in this study.

PHASE DIAGRAMS

The important phases in these rocks include hornblende, augite, orthoamphibole(s), ilmenite, cummingtonite, magnetite, biotite, plagioclase, garnet, quartz, orthopyroxene, and metamorphic fluid. These can be adequately described by the chemical components SiO_2, TiO_2, Fe_2O_3, FeO, MnO, MgO, CaO, Al_2O_3, Na_2O, K_2O,

and H_2O. The various phases can be projected in terms of many of these components of the AFMNCS system onto a modified AFM plane, with plagioclase (as albite and anorthite components), metamorphic fluid, ± quartz as the phases from which projections are made (Fig. 3).

The AFM plotting parameters in Figure 3 are modified after those of Robinson et al. (1982a, their Fig. 87). Na_2 and Ca are subtracted from Al_2 as required by projection from the respective albite and anorthite components. Fe_2^{3+} and Ti are added to Al_2 as important R^{3+} components and are not eliminated by projection from ilmenite and hematite because ilmenite does not occur in many samples and hematite, as a discrete phase, does not occur at all. Ti in amphibole is strongly correlated with Fe, apparently substituting largely as an ilmenite component by the coupled substitution $Fe^{2+} + Ti \leftrightharpoons 2R^{3+}$. This substitution requires the subtraction of one Fe^{2+} from the F corner for each Ti. Finally, Mn^{2+} is added to Fe^{2+}. Clearly the AFM projection in Figure 3 is a simplification of the natural system. One problem with this projection is that the effect of Na/(Na + Ca) ratios in amphibole and plagioclase on the phase relations cannot be examined. However, except as discussed below, no systematic effect of Na/(Na + Ca) ratios on amphibole phase relations in these rocks is evident (Hollocher, 1985). A more serious problem is that, although silica is omitted by projection from quartz for minerals in quartz-bearing assemblages, silica is simply ignored for minerals in quartz-free assem-
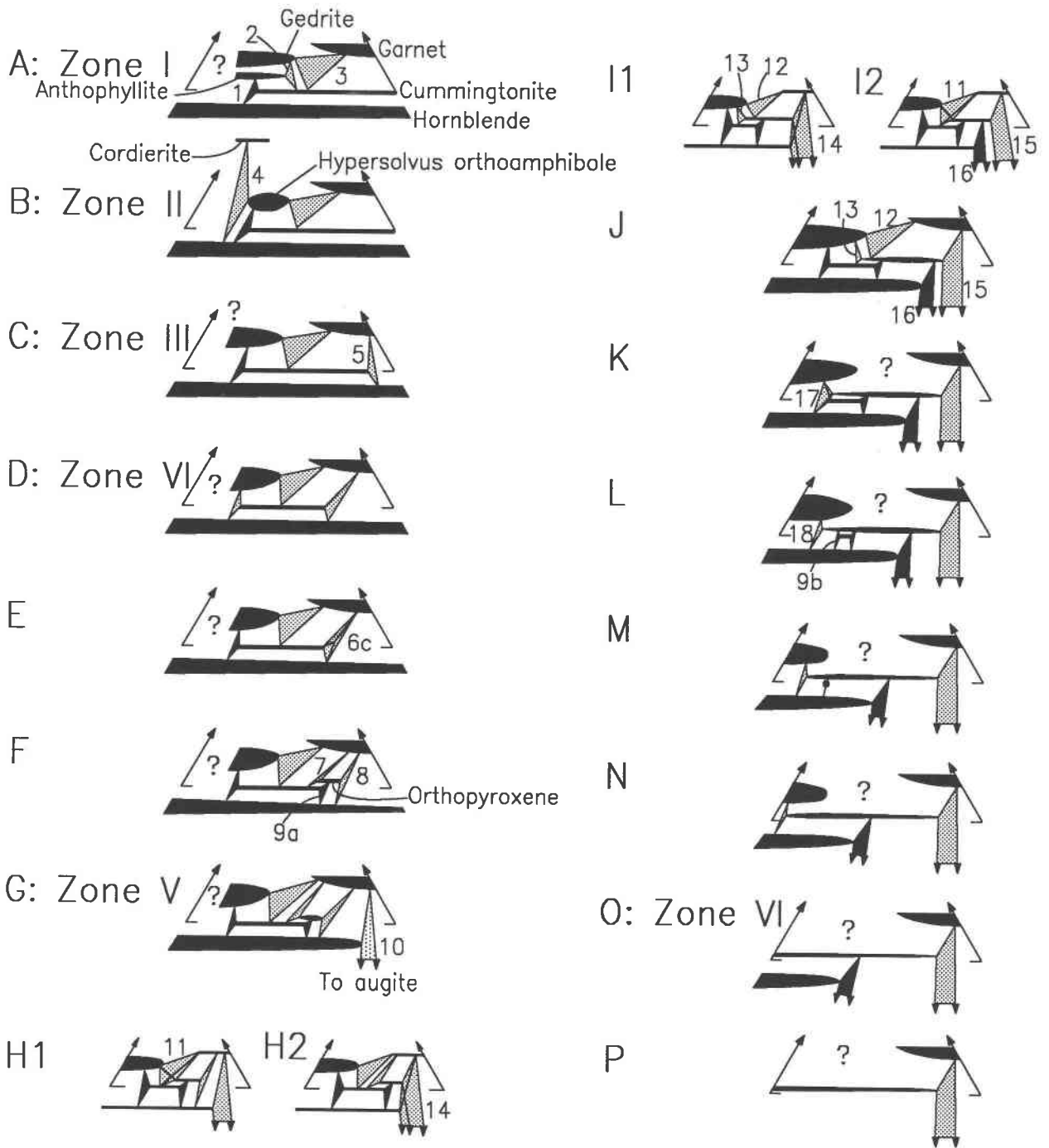
Fig. 4.   Schematic summary of the phase relations in quartz-bearing mafic rocks, shown in AFM projection (see Fig. 3 for plotting parameters). The schematic sequence of phase relations increases in metamorphic grade from Zone I (A) to Zone VI (P). Three-phase fields well constrained by the data are shown in black, and other fields, less well constrained, are stippled. Note that many parts of these diagrams are speculative.

blages in which the activity of silica can vary widely. Differences in silica activity can result in phase relations that are different from equivalent quartz-bearing assemblages, and allowances for these differences have to be made.

Despite the oversimplifications of the AFM projection, it serves to illustrate the phase relations in these rocks quite well. The assemblages and reactions discussed below are based on assemblages and textures observed in thin section, analyzed mineral compositions, and a de-

tailed analysis of a variety of phase diagrams (Hollocher, 1985). Reactions were checked and balanced using a least-squares program written after the method of Bryan et al. (1969), but reaction coefficients are omitted below because they depend on the actual mineral compositions used and thus have no general applicability.

PROGRADE METAMORPHIC REACTIONS

Although the data in Figure 3 have been separated by metamorphic zone, the data appear chaotic because of the progression of reactions in the same zone, complex solid solutions, uncertainties in the Fe^{3+} corrections, limitations of the projection, and differences in mineral assemblage. However, the data in Figure 3 can be interpreted in terms of a systematic progression of reactions with increasing metamorphic grade. The partly hypothetical phase relations and reactions for quartz-bearing rocks discussed below are summarized schematically in Figure 4.

Figure 4A shows the phase relations in Zone I, modified after Robinson et al. (1982a, their Fig. 87). At Mg-rich compositions there is a three-amphibole field representing a cummingtonite-forming continuous reaction that has been observed at this grade:

$$Ant + Hbl + Ilm + Qtz = Cum + Plag + Rut + H_2O \quad (1)$$
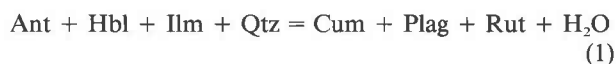
(Fig. 4A). This three-amphibole assemblage has not yet been found in Zone II, but it is constrained to occur at $M/(M + F)$ ratios of about 0.65, between quartz-bearing assemblages in Zone II containing cummingtonite + hornblende and orthoamphibole + hornblende at $M/(M + F)$ ratios of 0.6–0.75 (Fig. 3A). Similarly, quartz-bearing assemblages of anthophyllite + cummingtonite and cummingtonite + hornblende in Zone IV indicate that the three-amphibole assemblage in Reaction 1 occurs at $M/(M + F)$ ratios of 0.65 or greater (Fig. 3B).

The anthophyllite-gedrite solvus is apparently open in Zone I (Robinson et al., 1971b). Because cummingtonite coexists with garnet in intermediate to Fe-rich compositions even in Zone II (Fig. 3A; Huntington, 1975), a three-phase field containing cummingtonite + anthophyllite + gedrite may occur above the F-M join, representing the reaction

$$Ged + Cum + Qtz = Ant + Ilm + Plag + H_2O \quad (2)$$
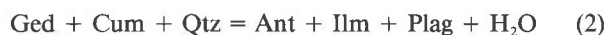
(Fig. 4A). A similar assemblage (but containing hornblende) from rocks of kyanite-staurolite grade in Vermont was reported by Spear (1982). If correct, then a three-phase field with gedrite, garnet, and cummingtonite must occur between the three-amphibole field of Reaction 2 and the garnet-cummingtonite tie line at more Fe-rich compositions, representing the reaction

$$Ged + An + Bio = Gar + Cum + Ab$$
$$+ Ilm + Qtz + H_2O \quad (3)$$
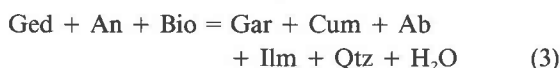
(Fig. 4A). This reaction defines an assemblage that is a subset of a similar assemblage reported by Spear (1982)

that contains hornblende and anthophyllite. The occurrence of the three-phase field with gedrite, cummingtonite, and garnet in Massachusetts is further indicated by a garnet-gedrite tie line in Zone I (Robinson et al., 1982a, their Fig. 87), which requires a three-phase field with gedrite and garnet below the tie line. Reaction 3 can be constrained in Zone II to lie on the Fe-rich side of gedrite + garnet (sample I34I of Robinson and Jaffe, 1969) and hornblende + orthoamphibole assemblages, and on the Mg-rich side of garnet + cummingtonite assemblages (Figs. 3A and 3B). Cummingtonite-staurolite tie lines that are chemically equivalent to the assemblage defined by Reaction 3 have not been found.

Although the orthoamphibole solvus is apparently closed by Zone II (Fig. 4B; Robinson and Jaffe, 1969; Robinson et al., 1971b), Robinson et al. (1982a, their Fig. 100) suggest that the solvus may still be open (reopened?) in Zone VI because of extra components in gedrite. This idea is based on their interpretation of textures in a rock from Zone VI, in which brown gedrite encloses blades of anthophyllite that are oriented parallel to the gedrite c axis. They interpret this texture as a coexisting prograde pair. My interpretation of similar textures in sample 77 from the same outcrop is that the anthophyllite blades are large, possibly recrystallized exsolution lamellae. In either case, complications surrounding the solvus will not be considered further.

Very Mg-rich rocks in Zone II with sufficient Al have assemblages of hornblende + orthoamphibole + cordierite (Schumacher and Robinson, 1987), possibly representing the reaction

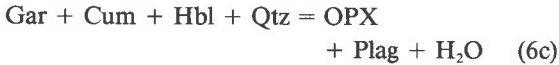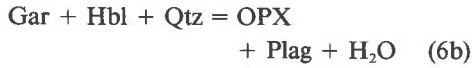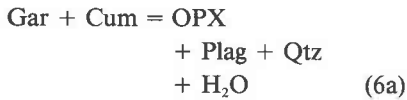$$Cord + Hbl + Qtz = Oam + Plag + Ilm + Bio + H_2O \quad (4)$$
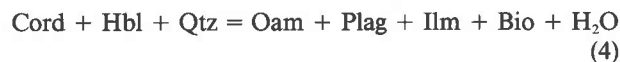
(Fig. 4B). Because this reaction probably proceeds to completion at the Mg sideline at higher grade in quartz-bearing rocks, it will not be considered further.

Huntington (1975) found cummingtonite with X_{Mg} as low as 0.172 in Zone II, and end-member iron cummingtonite at this or lower grade is possible. If so, cummingtonite breakdown probably began at the Fe sideline in Zone II or Zone III (Fig. 4C) because assemblages of cummingtonite + garnet + hornblende in place of Fe-rich cummingtonite are well established by Zone IV (Fig. 3B). This three-phase field represents the reaction

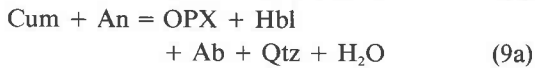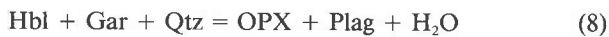$$Cum + Bio + Plag + Ilm = Hbl + Gar + Qtz + H_2O \quad (5)$$
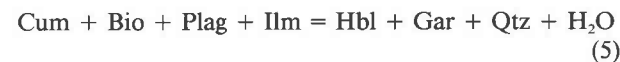
(Fig. 4C–4D). The initial breakdown of cummingtonite cannot involve very Fe-rich orthopyroxene, which is not stable relative to olivine + quartz at 6 kbar (e.g., Bohlen et al., 1983; Davidson and Lindsley, 1989). Orthopyroxene is first found in Zone V in amphibolites that have bulk X_{Mg} of about 0.4 (whole rock analyses in Hollocher, 1985). It is likely, however, that orthopyroxene first appears in AFM projection (Fig. 4E) at somewhat more Fe-rich compositions by way of three possible reactions:

$$Gar + Cum = OPX \quad\quad\quad\quad\quad\quad$$
$$+ Plag + Qtz \quad\quad\quad$$
$$+ H_2O \quad\quad (6a)$$
$$Gar + Hbl + Qtz = OPX \quad\quad\quad\quad$$
$$+ Plag + H_2O \quad (6b)$$
$$Gar + Cum + Hbl + Qtz = OPX \quad\quad$$
$$+ Plag + H_2O \quad (6c)$$

(Fig. 4E). Orthopyroxene appearing by either Reaction 6a or 6b requires colinearity (in projection) of the three phases garnet, orthopyroxene, and cummingtonite or garnet, orthopyroxene, and hornblende. Inspection of Figures 3A–3D shows that orthopyroxene-garnet and cummingtonite-garnet tie lines have shallow slopes compared to orthopyroxene-hornblende and cummingtonite-hornblende tie lines. Although the difference in the slopes of the tie lines is sensitive to the Fe^{3+} corrections, the marked differences in the slopes of the tie lines for many rocks imply that the colinearity needed for Reactions 6a and 6b is unlikely. Reaction 6c, in which orthopyroxene appears within the three-phase field of hornblende-cummingtonite-garnet is more likely correct.

In any case, Reaction 6c (or Reactions 6a or 6b by a more complex route) results in three new three-phase fields that represent the reactions

$$Cum + Gar = OPX + Plag + Qtz + H_2O \quad (7)$$

$$Hbl + Gar + Qtz = OPX + Plag + H_2O \quad (8)$$

$$Cum + An = OPX + Hbl \quad\quad\quad$$
$$+ Ab + Qtz + H_2O \quad (9a)$$

(Fig. 4F). An assemblage similar to that in Reaction 8 is found in sample 81 (Fig. 3D, with augite), and the assemblage defined by Reaction 9 is found in sample 74a (and 82 without quartz). Fe-rich hornblende must begin breaking down in Zone V or at lower grade. A likely reaction is

$$Hbl + Qtz = Gar + Aug + Plag + Bio + Ilm + H_2O$$
$$(10)$$
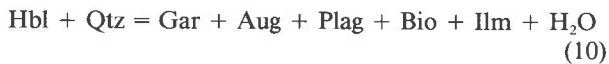
(Fig. 4G), which has not been found, but is a subset of the assemblage in sample 81 (Fig. 3D).

Current data obviously make it difficult to constrain the relative locations of many discontinuous reactions, particularly those above the F-M join where quartz-bearing assemblages are uncommon. One possibility is that Reaction 7, a dehydration reaction that proceeds toward higher X_{Mg} with increasing grade, first intersects Reaction 3 to produce the discontinuous reaction

$$Cum + Gar + Plag = Ged + OPX + H_2O \quad (11)$$

(Fig. 4H1). This reaction stabilizes assemblages of orthopyroxene + orthoamphibole and results in two new continuous reactions:

$$Oam + An + Qtz = OPX + Gar + Ab + H_2O \quad (12)$$

and

$$Oam + Cum = OPX + Plag + H_2O \quad (13)$$
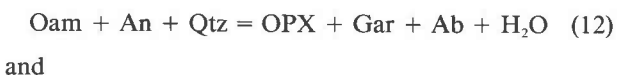
(Fig. 4I1). Quartz-free equivalents of Reaction 12 are found in Zones V and VI (Fig. 3C and 3D), but assemblages defined by Reaction 13 have not been found. The other possibility is that Reaction 8, which moves toward Fe-richer compositions with increasing grade, and Reaction 10, which moves toward Mg-richer compositions, intersect first, producing the discontinuous reaction

$$Hbl + Gar + Qtz = Aug + OPX + Plag + H_2O \quad (14)$$
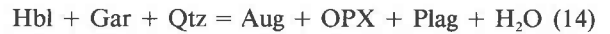
(Fig. 4H2), which defines an assemblage found in sample 81 (Fig. 3D) and occurring commonly in the Adirondacks (e.g., Jaffe et al., 1978). Reaction 14 produces two new continuous reactions:

$$Gar + Aug + Qtz = OPX + Plag \quad (15)$$

and

$$Hbl + Qtz = Aug + OPX + Plag + Ilm + Bio + H_2O$$
$$(16)$$
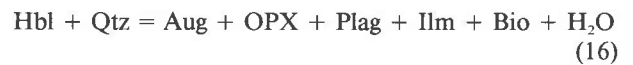
(Fig. 4I2). Both possible sequences in Figures 4H1 and 4I1 and 4H2 and 4I2 result in the same assemblages in Figure 4J. The three-phase field of Reaction 15 separates assemblages of garnet + augite on the Fe-rich side from orthopyroxene-bearing assemblages on the Mg-rich side. The assemblage for Reaction 15 involves only anhydrous minerals and probably moves little with increasing temperature.

Reaction 16 is probably the terminal reaction for hornblende in quartz-bearing rocks. An analysis of plagioclase compositions involved with this reaction indicates that the most stable hornblende in Reaction 16 at intermediate X_{Mg} has a Ca/(Ca + Na) ratio of about 0.82 (Hollocher, 1985). This implies a reversal in partitioning of Ca/Na between coexisting hornblende and plagioclase, confirming the interpretations of Robinson et al. (1982a, their Figs. 107–108) and Stoddard (1985).
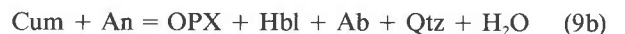
Reaction 13 proceeds toward higher X_{Mg} with increasing grade, and probably intersects Reaction 1 in lower Zone VI producing the discontinuous reaction

$$Oam + Cum + Plag = OPX + Hbl + Qtz + H_2O \quad (17)$$
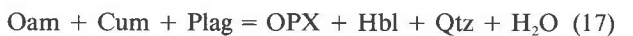
(Fig. 4K). This postulated reaction produces two new continuous reactions:

$$Oam + Hbl + Qtz = OPX + Plag + H_2O \quad (18)$$

and

$$Cum + An = OPX + Hbl + Ab + Qtz + H_2O \quad (9b)$$

(Fig. 4L). Reaction 18 probably proceeds to the Mg sideline, eliminating hornblende-orthoamphibole tie lines. Reaction 9b is a second reaction consuming cummingtonite identical to Reaction 9a, but proceeding in the opposite direction toward lower X_{Mg} with increasing grade (discussed in more detail below). Reactions 9a and 9b intersect (Fig. 4M), destroying the last bit of cummingtonite at intermediate compositions. This terminal cummingtonite composition requires colinearity (in projection) of hornblende, cummingtonite, and orthopyroxene, which may be a consequence of crystal chemical con-

straints that stabilize cummingtonite of intermediate composition (see below).

Based on current data, the highest grade rocks in southern New England yield assemblages shown in Figure 4O. At higher metamorphic grade, Reaction 16 is expected to go to completion at the Mg sideline, leaving the assemblages shown in Figure 4P.

REACTIONS IN T-X_{Mg} SPACE

The occurrence and locations of Reactions 1, 9, and 16, all involving quartz, are reasonably well constrained by chemical data in Figure 3. By combining these compositional constraints with estimated prograde metamorphic temperatures (Table 1), an attempt has been made to locate these reactions in T-X_{Mg} space. Figure 5 is a set of T-X_{Mg} diagrams that are approximately isobaric (about 6 kbar) sections made through the AFM composition field between hornblende and the F-M join in the projections of Figure 4.

In Figure 5A, the Fe-Mg reaction loop for Reaction 1 (producing cummingtonite) is constrained by the compositions of orthoamphibole in assemblages of hornblende + orthoamphibole on the high X_{Mg}, low temperature side, and by cummingtonite compositions in assemblages of hornblende + cummingtonite on the low X_{Mg}, high temperature side. The reaction loop must also lie at higher X_{Mg} or lower temperature than those conditions appropriate for cummingtonite in assemblages of cummingtonite + garnet and cummingtonite + orthopyroxene. The reaction loop is closely constrained by an assemblage of cummingtonite + hornblende on the Fe-rich side (sample 65a) and an anthophyllite + hornblende assemblage on the Mg-rich side (sample 65b). Samples N, 62, 64, and 72 contain the quartz-free reaction assemblage. Because quartz is on the left side of Reaction 1, the equivalent quartz-absent reaction should occur at higher temperature or at more Fe-rich compositions. Indeed, samples N, 64, and 72 do lie at higher temperatures than the estimated position of the quartz-present loop for Reaction 1. The quartz-bearing assemblage of hornblende + orthopyroxene in sample 79 suggests that the Reaction 1 loop either lies at lower temperatures or higher X_{Mg} than that sample.

In Figure 5B the Fe-Mg loop for Reaction 9a, which consumes cummingtonite, is largely constrained on the high X_{Mg}, low temperature side by cummingtonite compositions in cummingtonite + hornblende assemblages and on the low X_{Mg}, high temperature side by orthopyroxene compositions in orthopyroxene + hornblende assemblages. The reaction loop must also lie at lower X_{Mg} or higher temperature than conditions appropriate for assemblages of hornblende + orthoamphibole, and at higher X_{Mg} or lower temperature than conditions appropriate for assemblages of hornblende + orthopyroxene + augite. Note that the Reaction 9a assemblage occurs in sample 74a. Because quartz occurs on the right side of Reaction 9a, the equivalent quartz-absent reaction should occur at lower temperature or higher X_{Mg}, explaining why the quartz-free reaction assemblage in sample 82 lies be-
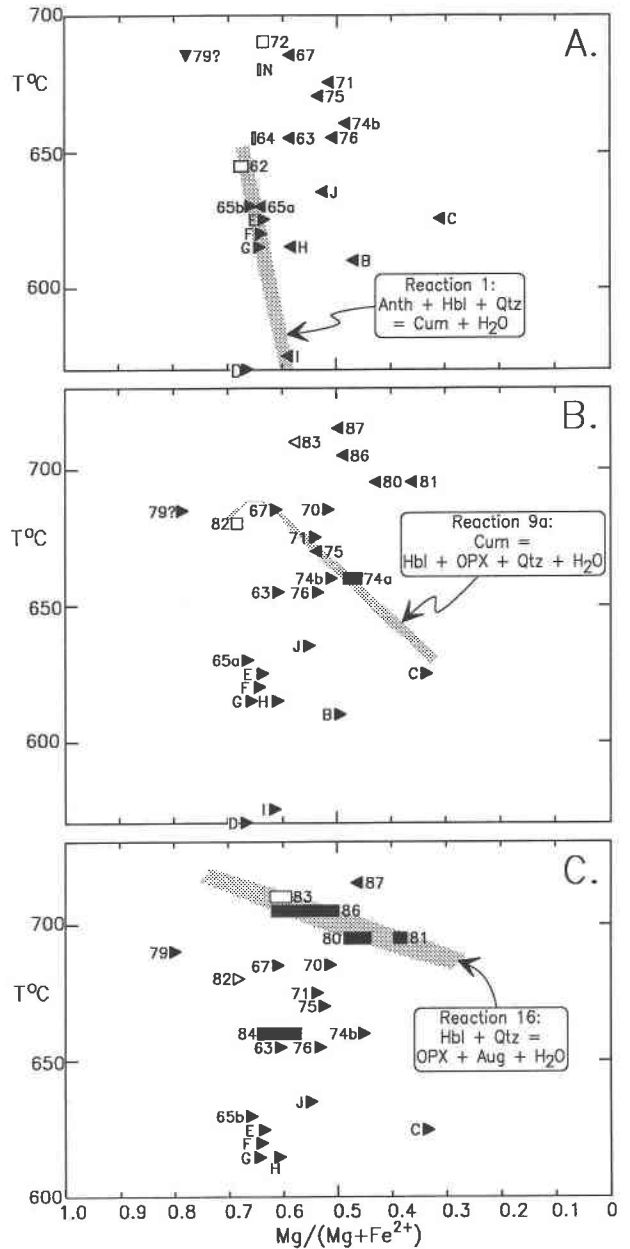

Fig. 5. T-X_{Mg} diagrams showing the assemblages that constrain Fe-Mg loops for Reactions 1 (**A**), 9a (**B**), and 16 (**C**). The best locations for the reaction loops are stippled. Symbols for quartz-bearing assemblages are closed, and symbols for equivalent quartz-free assemblages are open. Triangles point toward the likely location of the reaction loops. Rectangles represent assemblages that define the actual reaction loop.

low the estimated position of the quartz-present reaction loop. The extrapolation of the reaction loop yields higher temperatures than those appropriate for the quartz-bearing assemblage of hornblende + orthopyroxene in sample 79 at an X_{Mg} of 0.79. Because the assemblage defined by Reaction 9a should occur at lower temperatures than the assemblage found in sample 79, the reaction loop either ends in a discontinuous reaction below about 685 °C (no
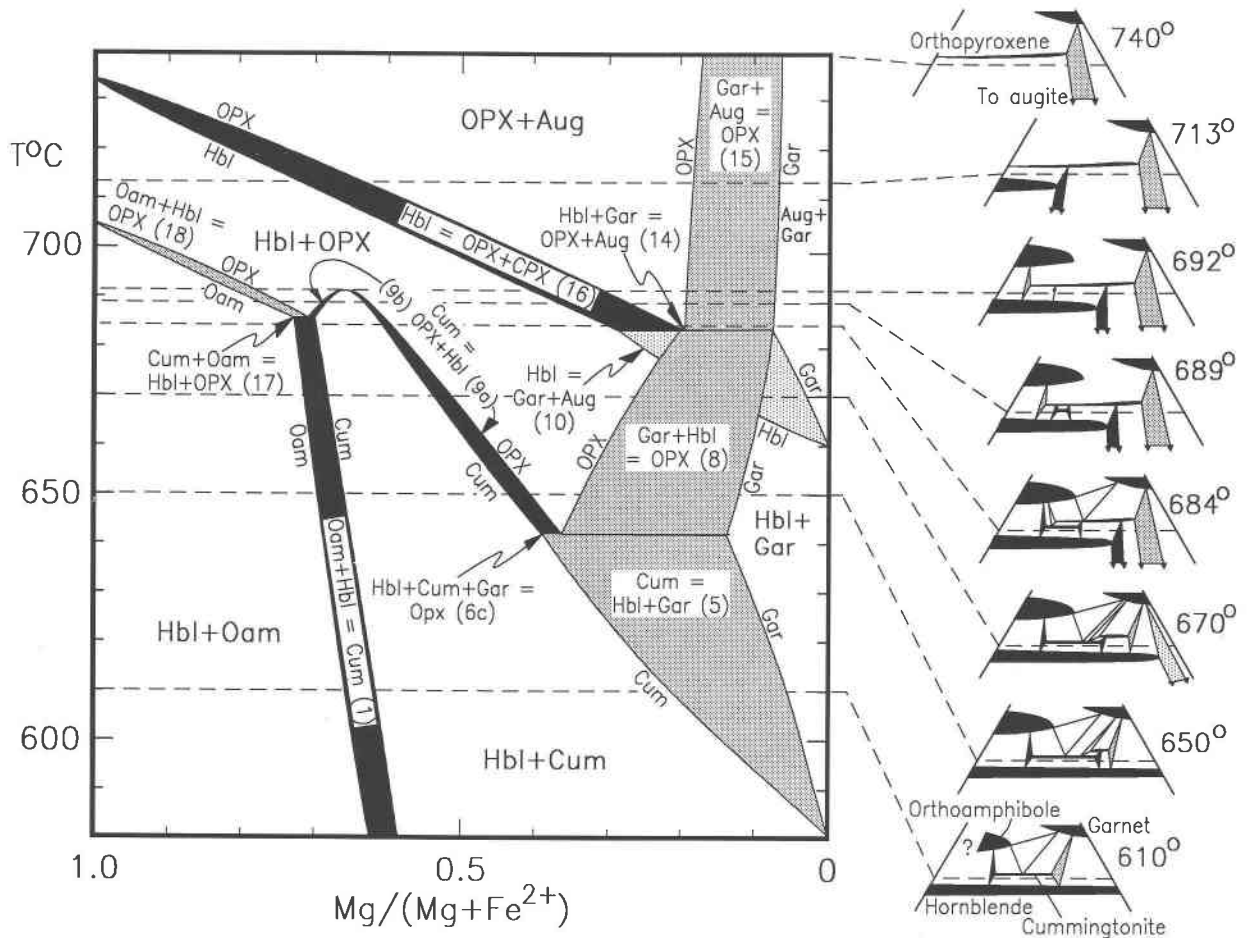
Fig. 6. Summary T-X_{Mg} diagram showing an approximately isobaric (6 kbar) pseudosection through the AFM projection between the F-M join and the composition field of hornblende. Three-phase fields of continuous reactions appear as Fe-Mg reaction loops, and discontinuous reactions appear as horizontal lines that terminate loops. The sides of the loops represent the compositions of minerals that are involved in the loop reaction, labeled adjacent to the limb of each loop. The two-phase fields and three- and four-phase reaction assemblages are also labeled, and reaction numbers from the text are given in parentheses. Reactions 1, 9a, 9b, and 16 are shown black, other reactions in the plane of the T-X_{Mg} section are stippled, and reactions out of the plane of section are open (see Fig. 3 for AFM plotting parameters). Relative estimated temperatures are probably fairly precise, but they should not be considered accurate to better than ± 50 °C.

evidence), or the loop crests at a temperature maximum at intermediate compositions with Reaction 9b on the Mg-rich side of the crest (as suggested above).

In Figure 5C the Fe-Mg loop for Reaction 16, which consumes hornblende, is constrained on the high X_{Mg}, low temperature side by hornblende compositions in augite-free assemblages of hornblende + orthopyroxene and in assemblages containing cummingtonite and orthoamphibole. On the low X_{Mg}, high temperature side, the loop is constrained by orthopyroxene compositions in the hornblende-free two pyroxene granulite of sample 87. The quartz-bearing reaction assemblage occurs in samples 80, 81, 84, and 86. Unfortunately, sample 84 is located at an anomalously low temperature. However, the isotherms used to estimate the prograde temperature for sample 84

(Fig. 1B) are poorly constrained in the area of sample 84 (and 85) and are probably in error relative to the other samples.

DISCUSSION

The analysis given above and in Figure 5 is admittedly crude. However, the observed mineral assemblages and compositions (Fig. 3), the partly hypothetical framework of phase relations (Fig. 4), and the three T-X_{Mg} reaction loops located approximately (Fig. 5) can be interpreted in terms of a T-X_{Mg} phase diagram that is internally consistent for quartz-saturated rocks in Zones II–VI that lie in AFM projection between the F-M join and the field or hornblende solution (Fig. 6).

In Zone II (Fig. 6, about 580 °C), the area between the

F-M join and hornblende in AFM projection is dominated by two-phase fields of hornblende + orthoamphibole and hornblende + cummingtonite, separated by the three-phase field of orthoamphibole + hornblende + cummingtonite of continuous Reaction 1.

Garnet first appears in Figure 6 by Reaction 5 at the Fe sideline at a temperature schematically shown as 580 °C. With increasing temperature, garnet coexists with increasingly Mg-rich rocks as cummingtonite breaks down. At higher temperatures orthopyroxene appears at the expense of orthoamphiboles and cummingtonite by several different reactions (6, 8, 9, 17, 18), depending on the X_{Mg} of the rock, to produce orthopyroxene-bearing amphibolites. Garnet with, or in place of, orthopyroxene persists in more Fe-rich rocks.

Hornblende starts being lost in Figure 6 by Reaction 10, which probably begins at the Fe sideline at a temperature schematically shown at 660 °C. At the highest temperatures in Figure 6, orthopyroxene + augite assemblages form by Reactions 14, 15, and 16, depending on the rock composition, to produce the granulite assemblages of two pyroxene ± garnet common in Zone VI.

The reactions, assemblages, and mineral compositions will differ from those described above under other metamorphic conditions. For example, considering only rocks with assemblages of orthopyroxene + augite ± hornblende, metamorphism at 6 kbar in central Massachusetts allowed garnet to coexist with orthopyroxene having X_{Mg} up to about 0.4. Jaffe et al. (1983) report garnet coexisting with orthopyroxene having X_{Mg} up to 0.55 at pressures estimated at 8–10 kbar in similar assemblages from the Adirondacks. In contrast, Russ-Nabelek (1989) reported no garnet in a variety of mafic rocks metamorphosed at pressures near 3 kbar.

CONCLUSIONS

Mafic rocks in central Massachusetts were metamorphosed at lower sillimanite grade (Zone II) to produce a variety of assemblages, including quartz- and plagioclase-bearing hornblende, hornblende + cummingtonite, hornblende + orthoamphibole, and hornblende + orthoamphibole + cummingtonite. These assemblages evolved by a series of reactions with increasing grade that systematically transformed amphibolites into granulites containing two pyroxene ± garnet. For subaluminous mafic rocks with intermediate X_{Mg} containing quartz and plagioclase, the reaction sequence can be simplified and described in terms of a series of metamorphic assemblages: hornblende + orthoamphibole (Mg-rich rocks only), hornblende + cummingtonite, hornblende + orthopyroxene, and orthopyroxene + augite. These assemblages are separated by boundary Reactions 1, 9, and 16, respectively. This assemblage series occurs over an estimated temperature range of 580–730 °C.

ACKNOWLEDGMENTS

REFERENCES CITED

Berry, Henry, IV (1988) Possible correlations of pre-Silurian basement in the Merrimack belt, south-central Massachusetts. Geological Society of America Abstracts with Programs, 20, 6.

Bohlen, S.R., Wall, V.J., and Boettcher, A.L. (1983) Geobarometry in granulites. In S.K. Saxena, Ed., Kinetics and equilibrium in mineral reactions, p. 141–171. Springer-Verlag, New York.

Bryan, W.B., Finger, L.W., and Chayes, Felix (1969) Estimating proportions in petrographic mixing equations by least-squares approximation. Science, 123, 926–927.

Davidson, P.M., and Lindsley, D.H. (1989) Thermodynamic analysis of pyroxene-olivine-quartz equilibria in the system CaO-MgO-FeO-SiO₂. American Mineralogist, 74, 18–30.

Dymek, R.F. (1983) Titanium, aluminum and interlayer cation substitutions in biotite from high-grade gneisses, West Greenland. American Mineralogist, 68, 880–899.

Hollocher, Kurt (1981) Retrograde metamorphism of the Lower Devonian Littleton Formation in the New Salem area, west-central Massachusetts, 268 p. M.S. thesis, University of Massachusetts, Amherst, Massachusetts.

——— (1984) Hornblende, cummingtonite, and gedrite breakdown reactions in the eastern Acadian metamorphic high, south-central Massachusetts and northern Connecticut. Geological Society of America Abstracts with Programs, 16, 25.

——— (1985) Geochemistry of metamorphosed volcanic rocks in the Middle Ordovician Partridge Formation and amphibole dehydration reactions in the high-grade metamorphic zones of central Massachusetts, 275 p. Ph.D. thesis, University of Massachusetts, Amherst, Massachusetts.

Huntington, J.C. (1975) Mineralogy and petrology of metamorphosed iron-rich beds in the Lower Devonian Littleton Formation, Orange area, Massachusetts, 106 p. M.S. thesis, University of Massachusetts, Amherst, Massachusetts.

Jaffe, H.W., Robinson, Peter, and Klein, Cornelis (1968) Exsolution lamellae and optic orientation of clinoamphiboles. Science, 160, 776–778.

Jaffe, H.W., Robinson, Peter, Tracy, R.J., and Ross, Malcolm (1975) Orientation of pigeonite exsolution lamellae in metamorphic augite. Correlation with composition and calculated optimal phase boundaries. American Mineralogist, 60, 9–28.

Jaffe, H.W., Robinson, Peter, and Tracy, R.J. (1978) Orthoferrosilite and other iron-rich pyroxenes in microperthite gneiss of the Mount Marcy area, Adirondack Mountains. American Mineralogist, 63, 1116–1136.

Jaffe, H.W., Jaffe, E.B., Ollila, P.W., and Hall, L.M. (1983) Bedrock geology of the High Peaks region, Marcy Massif, Adirondacks, New York, 78 p. Friends of the Grenville Field Trip Guidebook, University of Massachusetts, Amherst, Massachusetts.

Laird, Jo (1980) Phase equilibria in mafic schist from Vermont. Journal of Petrology, 21, 1–37.

Robinson, Peter (1983) Realms of regional metamorphism in southern New England, with emphasis on the eastern Acadian metamorphic high. In P.E. Schenk, Ed., Regional trends in the geology of the Appalachian-Caledonian-Hercynian-Mauritanide Orogen, p. 249–258. Reidel, The Netherlands.

Robinson, Peter, and Jaffe, H.W. (1969) Chemographic exploration of amphibole assemblages from central Massachusetts and southwestern New Hampshire. In J.J. Papike, Ed., Pyroxenes and amphiboles: Crystal chemistry and phase petrology. Mineralogical Society of America, Special Publication 2, 251–274.

Robinson, Peter, and Tracy, R.J. (1979) Gedrite-cordierite, gedrite-orthopyroxene assemblages from ferromagnesian gneisses, sillimanite–K-feldspar zone, central Massachusetts. Geological Society of America Abstracts with Programs, 11, 504.

Robinson, Peter, Jaffe, H.W., Klein, Cornelis, Jr., and Ross, Malcolm

(1969) Equilibrium coexistence of three amphiboles. Contributions to Mineralogy and Petrology, 22, 248–258.

Robinson, Peter, Jaffe, H.W., Ross, M., and Klein, C. (1971a) Orientations of exsolution lamellae in clinopyroxenes and clinoamphiboles: Consideration of optimal phase boundaries. American Mineralogist, 56, 909–939.

Robinson, Peter, Ross, Malcolm, and Jaffe, H.W. (1971b) Composition of the anthophyllite-gedrite series, comparisons of gedrite and hornblende, and the anthophyllite-gedrite solvus. American Mineralogist, 56, 1005–1041.

Robinson, Peter, Ross, M., Nord, G.L., Jr., Smyth, J.R., and Jaffe, H.W. (1977) Exsolution lamellae in augite and pigeonite: Fossil indicators of lattice parameters at high temperature and pressure. American Mineralogist, 62, 857–873.

Robinson, Peter, Spear, F.S., Schumacher, J.C., Laird, Jo, Klein, Cornelis, Evans, B.W., and Doolan, B.L. (1982a) Phase relations of metamorphic amphiboles: Natural occurrence and theory. In Mineralogical Society of America Reviews in Mineralogy, 9B, 1–227.

Robinson, Peter, Tracy, R.J., Hollocher, Kurt, and Dietch, C.W. (1982b) High grade Acadian regional metamorphism in south-central Massachusetts. In R. Joesten and S.S. Quarrier, Eds., New England intercollegiate geological conference guidebook, 74th Annual Meeting, p. 289–339. Storrs, Connecticut.

Robinson, Peter, Tracy, R.J., Hollocher, Kurt, Schumacher, John, and Berry, H.N., IV (1986) The central Massachusetts metamorphic high. In Peter Robinson and D.C. Elbert, Eds., Regional metamorphism and metamorphic phase relations in northwestern and central New England. International Mineralogical Association Field Trip Guidebook, Trip B-5, p. 195–284. University of Massachusetts, Amherst, Massachusetts.

Robinson, Peter, Tucker, R.D., and Hollocher, Kurt (1989) The nature of the Bronson Hill zone during the Taconian Orogeny. In Maurice Colpron and Barry Doolan, Eds., Proceedings of the Quebec-Vermont Appalachian Workshop, University of Vermont, Burlington, Vermont, 26–28.

Russ-Nabelek, C. (1989) Isochemical contact metamorphism of mafic schist, Laramie Anorthosite Complex, Wyoming: Amphibole compositions and reactions. American Mineralogist, 74, 530–548.

Schumacher, John (1983) Stratigraphic, geochemical, and petrologic studies of the Ammonoosuc Volcanics, north-central Massachusetts and southwestern New Hampshire, 237 p. Ph.D thesis, Massachusetts, Amherst, Massachusetts.

Schumacher, John, and Robinson, Peter (1987) Mineral chemistry and metasomatic growth of aluminous enclaves in gedrite-cordierite-gneiss from southwestern New Hampshire, USA. Journal of Petrology, 28, 1033–1073.

Spear, F.S. (1978) Petrogenetic grid for amphibolites from the Post Pond Volcanics, Vermont. Carnegie Institution of Washington Year Book, 77, 805–808.

——— (1980) The gedrite-anthophyllite solvus and the composition limits of orthoamphibole from the Post Pond Volcanics, Vermont. American Mineralogist, 65, 1103–1118.

——— (1982) Phase equilibria of amphibolites from the Post Pond Volcanics, Mt. Cube Quadrangle, Vermont. Journal of Petrology, 23, 383–426.

Stoddard, E.F. (1985) Zoned plagioclase and the breakdown of hornblende in pyroxene amphibolites. Canadian Mineralogist, 23, 195–204.

Tracy, R.J., Robinson, Peter, and Thompson, A.B. (1976) Garnet composition and zoning in the determination of temperature and pressure of metamorphism, central Massachusetts. American Mineralogist, 61, 762–775.

Wolff, R.A. (1978) Ultramafic lenses in the Middle Ordovician Partridge Formation, Bronson Hill anticlinorium, central Massachusetts, 162 p. M.S. thesis, University of Massachusetts, Amherst, Massachusetts.

Zen, E-An, Ed. (1983) Bedrock geologic map of Massachusetts, 1:250,000. U.S. Geological Survey, 3 sheets.

APPENDIX 2.   Samples used from other studies

This paper	Original sample no.	Metamorphic zone
A	6A9X	Zone II
B	7A8BX	Zone II
C	2J14	Zone II
D	J87D	Zone II
E	155	Zone II
F	T59B	Zone II
G	K44C	Zone II
H	K44E	Zone II
I	498	Zone II
J	Q795	Zone II
K	N30X	Zone III
L	NO1A	Zone III
M	K34A	Zone IV
N	QB27C	Zone IV

Samples A–K and N are from Robinson and Jaffe (1969), sample C is from Huntington (1975), and samples L and M are from Wolff (1978).